



# Exploring the boundaries of refill friction stir spot welding: influence of short welding times on joint performance

Jonathan Draper<sup>1</sup> · Sebastian Fritsche<sup>2</sup> · Andrew Garrick<sup>1</sup> · Sergio T. Amancio-Filho<sup>2</sup> · Athanasios Toumpis<sup>1</sup> · Alexander Galloway<sup>1</sup>

Received: 10 October 2023 / Accepted: 9 February 2024  
© The Author(s) 2024

## Abstract

Refill friction stir spot welding is a solid-state spot-welding technique suited to lap joining of thin aluminium sheets, including difficult-to-weld 2xxx series alloys that are prone to hot cracking during fusion welding processes. Long welding time is an ongoing challenge that hinders industrial adoption of the process. To address this, the present study explores much shorter welding times than those previously reported in the literature and assesses the impact on joint quality. Joints of 1.8 mm thick AA2024-T3 sheet were produced with welding times from 3 s, down to 0.75 s and rotational speeds of 1000 rpm to 2500 rpm. Defect formations within the welds were studied with the aid of optical microscopy. The mechanical properties were evaluated using tensile lap shear testing and microhardness mapping, and failure modes were characterised using scanning electron microscopy. Various weld defects were found at all welding times and rotational speeds, and the defects enlarged with decreasing welding time and increasing RS. The highest lap shear strength of 9.21 kN was achieved with a welding time of 3 s and rotational speed of 2000 rpm; lap shear strengths of 7.02 kN and 6.37 kN were achieved for 1.5 s and 0.75 s welds, respectively.

**Keywords** Refill friction stir spot welding · Friction welding · Solid-state joining · Aluminium alloys · Aerospace materials

## 1 Introduction

Refill friction stir spot welding (RFSSW) is a solid-state friction welding process derived from the widely established friction stir welding technology and has drawn increasing attention from research and industrial bodies as an alternative to conventional spot joining processes. Competitor technologies include resistance spot welding, mechanical fasteners (bolts, rivets, clinching, etc.), as well as fusion-based spot welding (arc, beam). As a solid-state process, RFSSW offers the advantages of reduced heat input, lower

thermal distortion, no need for filler material, and reduced energy costs compared with fusion welding and resistance spot welding [1–3]. Another advantage is the ability to join alloys with poor weldability, such as 2xxx and 7xxx series aluminium [4–6], without the risk of solidification cracking associated with fusion welding processes [7, 8]. As a replacement for rivets and bolts, the process offers mass saving benefits, as no additional material is added, and reduces the risk of galvanic corrosion which poses an ongoing challenge in aerospace design [1, 9].

As discussed comprehensively in multiple reviews [10, 11], much research to date has addressed the influence of the process parameters, namely tool rotational speed (RS), plunge depth and welding time. The predominant focus of past research [10, 11] has been to optimise welding parameters for maximum ultimate lap shear force (ULSF) (typically in the range of 6–10 kN), without consideration for the requirements of industrial users, such as production rate. Welding time, the time taken to complete the plunge and refill stages of the RFSSW cycle, presents a challenge when considering the widespread adoption of the process in mass manufacturing industries [12, 13]. As a key competitor for

---

Recommended for publication by Commission III—Resistance Welding, Solid State Welding, and Allied Joining Process

---

✉ Jonathan Draper  
jonathan.draper@strath.ac.uk

<sup>1</sup> Department of Mechanical & Aerospace Engineering, University of Strathclyde, Glasgow, UK

<sup>2</sup> Institute of Materials Science, Joining and Forming, Graz University of Technology, BMK Endowed Professorship for Aviation, Graz, Austria

RFSSW, resistance spot welding provides a useful comparison in terms of welding time, requiring roughly 1–2 s per weld [14]; RFSSW should match or improve on this to be a competitive joining technology for high production rate applications. A limited number of studies have shown that welding times of around 2 s are achievable for automotive aluminium alloys such as 5xxx and 6xxx series [13, 15–17]. However, little is known about applying such short welding times to aerospace alloys, such as the 2xxx series, with the vast majority of literature for these alloys addressing welding times greater than 5 s [18–27]. The shortest welding time for a 2xxx series RFSSW joint was reported by de Castro et al. [28], who reached as low as 3 s. The present study addresses this knowledge gap by exploring significantly shorter RFSSW welding times for AA2024-T3 joints, down to 0.75 s.

The adverse relationship between welding time and formation of weld defects has been previously reported [2, 29]. Shang et al. [29] investigated welds of 2 mm thick AA2060-T8 with weld times of 4.8–6 s and RS of 2500 rpm. A maximum ULSF of 5.71 kN was achieved and cavity defects were observed within the welds, characteristic of poor material flow into the shoulder region of the weld. The authors [29] concluded that voids do not meaningfully influence the ULSF, which is instead influenced by the hook morphology. A study by da Silva et al. [22] investigated welds of AA2024-T3 at a welding time of 3.8 s. The highest ULSF was achieved with a RS of 1900 rpm and 1700 rpm for the plunge and refill stages respectively, however, voids were still found to be present within the weld. Tier et al. [27] investigated joints of Alclad coated AA2024-T3 and concluded that higher ULSF is achieved at longer welding times (10.68 kN at 4.81 s). Amancio-Filho et al. [18] studied the influence of welding time and RS on AA2024-T3 joints. Varying the welding time from 4.8–6.8 s and RS from 1900–2900 rpm, the highest ULSF of 10.3 kN was achieved with the longest time and lowest RS. Parra et al. [30] studied joints of AA6181-T4 with welding time ranging from 2–3.4 s and RS of 1900–2900 rpm. The maximum ULSF was achieved with a welding time of 3 s, below which the ULSF decreased and the results became more scattered. It was concluded that welding times shorter than 3 s caused excessively high strain rates and the formation of defects [22]. Hovanski et al. [31] presented the only prior study of welding time reduction for aerospace series aluminium joints. The investigation assessed AA7075-T6

joints and showed that, using a 7 mm diameter shoulder, ULSF of 4.28 kN could be achieved with a welding time of 1 s and an RS of 3000 rpm. However, no micrographs of the resulting weld cross-sections were presented, and the presence of weld defects was not discussed.

The current study investigates AA2024-T3 RFSSW joints produced at significantly shorter welding times than have previously been reported in the literature, with the aim of increasing process readiness for high production rate manufacturing applications. Through exploration of the weld defects, microstructures, mechanical properties and failure modes, an understanding of the influence of short welding times on these characteristics is developed that will support future industrial uptake of the RFSSW process.

## 2 Experimental methodology

Chemical composition and mechanical properties of the workpiece base material are given in Table 1. Mechanical properties were established by tensile testing in accordance with BS EN ISO 6892-1:2019 [32], using an Instron 5969 universal testing machine. Welding was performed using an RPS100 RFSSW machine from Harms & Wende. All tool components were made from H13 tool steel, and their outer diameters were 18 mm, 9 mm and 6.4 mm for the clamping ring, shoulder, and pin, respectively (shown in Fig. 1b). A detailed discussion of tool geometry can be found in the work of Li et al. [33].

As detailed in Table 2, three welding times were selected to assess the influence on ULSF and defect formation. The shortest welding time of 0.75 s represents the upper speed limit of the welding machine tool actuators. The tool RS was also varied from 1000–2500 rpm to assess the influence of different heat inputs. The shoulder plunge depth was kept constant at 2.25 mm, equal to 1.25 times the top sheet thickness. This is broadly in line with the optimal plunge depth most often identified in the literature [22, 27]. The tool volume ratio (ratio of volume displaced by the plunging shoulder to the volume created by the retracting pin) was kept constant at 0.8. Table 2 details the full list of welding parameter sets investigated. A sample size of three was used for all parameter sets.

Weld samples were sectioned vertically through the weld centre, prepared to a final polish with 0.02  $\mu\text{m}$  OPS using a standard metallographic preparation process, and

**Table 1** Chemical composition and mechanical properties of AA2024-T3 [23, 34]

Chemical composition (wt%)										Mechanical properties		
Al	Si	Fe	Cu	Mn	Mg	Cr	Ni	Zn	Ti	Tensile strength (MPa)	Yield strength (MPa)	Elongation (%)
Bal	0.5	0.5	4.9	0.9	1.8	0.1	0.05	0.25	0.15	509	375.8	13.9

**Fig. 1** **a** Dimensions and configuration of welding samples (mm), **b** assembled welding tool, **c** sample holder jig

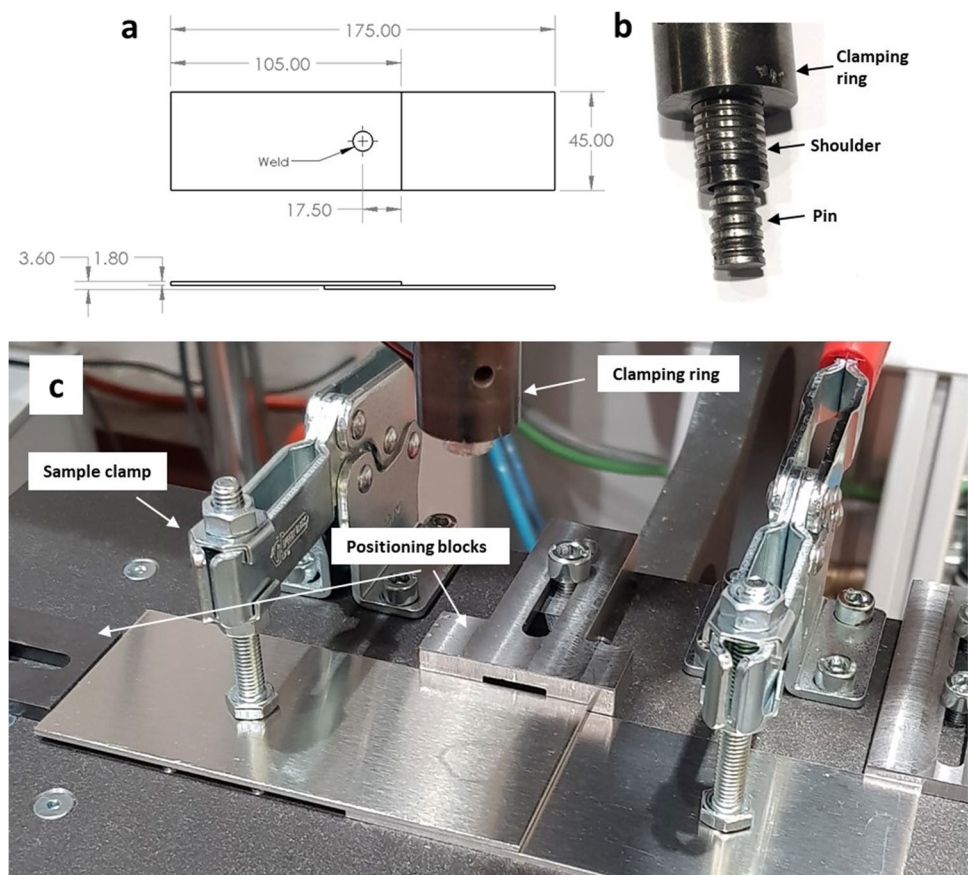


**Table 2** Welding parameters for sample production

Parameter ID	RS (rpm)	Welding time (s)	Plunge depth (mm)
P01	1000	3	2.25
P02	1500		
P03	2000		
P04	2500		
P05	1000	1.5	
P06	1500		
P07	2000		
P08	2500		
P09	1000	0.75	
P10	1500		
P11	2000		
P12	2500		

electro-etched using Barker's solution (20 ml HBF<sub>4</sub>, 80 ml H<sub>2</sub>O) for 120 s. The microstructure and defect formation of the welds were optically examined using a GX51 metallurgical microscope (Olympus).

To assess the influence of the welding process parameters on the hardness of the material throughout the welding region, Vickers microhardness maps were produced using

a Qness 60 A + Evo hardness tester (QATM), with 0.5 N load and 10 s dwell time, in accordance with BS EN ISO 6507-4:2018 [35]. Measurements were taken in a square grid pattern of 0.1 mm increments.

The ULSF of the joints was evaluated by single tensile lap shear testing using an Instron 5969 universal testing machine. The dimensions and weld configuration of the samples used are shown in Fig. 1a. A custom clamping jig (Fig. 1c) was used to ensure a consistent weld position, and 35 mm overlap between the top and bottom sheet for all samples. Samples were loaded with a crosshead speed of 2 mm/min until failure, in accordance with EN ISO 14273. Fractography of the failed joints was performed using a HITACHI S-3700N scanning electron microscope (SEM).

The ULSF of the weld samples can be compared with the acceptance criteria for competitor joining technologies. Elsewhere [36], it has been suggested that the resistance spot welding standard BS ISO 16338:2017 [37] provides an acceptable reference for the ULSF requirements of RFSSW joints. The standard states that, for 1.8 mm thick sheets of aluminium with a tensile strength greater than 386 MPa, spot welds should carry an average minimum ULSF of 4.605 kN [37]. A further comparison can be made with riveting; according to MMPDS-11 [38], the ULSF of a single



countersunk rivet joint for AA2024-T3 sheets of 1.8 mm thickness should reach a minimum of 7.27 kN.

### 3 Results & discussion

#### 3.1 Defect formation

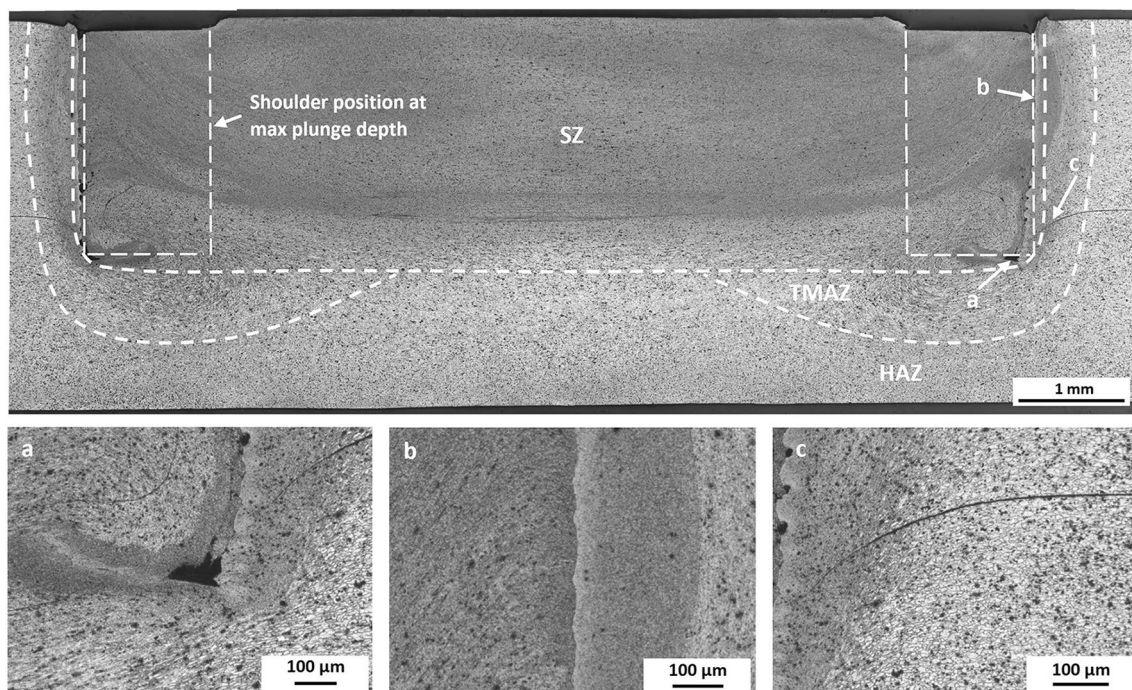
Figure 2 shows a micrograph of a RFSSW joint with several common defects. Incomplete refill (Fig. 2a) is associated with the loss of material through gaps between the tool components [39]. Lack of peripheral mixing (Fig. 2b) results from lack of mixing between the refilled material and the sidewall of the weld zone, typically indicating a lack of material flow due to insufficient heat input [40]. Tunnel defects (Fig. 2c) are circumferential voids that form near the outer edge of the shoulder/ workpiece interface. This defect occurs when insufficient heat input leads to poor material flow and an inability for the material to fully consolidate during the refill stage [2, 40]. A curved hook feature (Fig. 2d) occurs in the vast majority of RFSSW joints at the transition from bonded to unbonded workpiece material. Silva et al. [13] determined that the geometry of the hook is strongly influenced by the shoulder plunge depth and that it has a significant influence on mechanical performance of the joint.

Figure 3 presents micrographs of the shoulder plunge regions for each of the tested parameters. Due to insufficient heat input and material softening, welds could not be produced at welding times of 1.5 s or 0.75 s with RS of 1000 rpm as the torque required exceeded the welding machine limit.

#### 3.1.1 Tunnel defects

The presence of tunnel defects is clearly visible irrespective of welding parameters (Fig. 3), although their size and position are strongly influenced by welding time and RS. These defects are minimised at high welding time and low RS. At all welding times it was found that increasing RS led to a larger tunnel defect area. While this appears counterintuitive as higher RS naturally results in greater heat input, which may be expected to improve material flow, the additional heat generation at the tool/ material interface has been shown in other studies to promote slipping [41], resulting in localised mixing at the interface and reduced overall mixing in the stir zone (SZ). This is in agreement with the work of Shen et al. [2] and Rosendo et al. [42] who observed comparable results attributable to tool slippage.

At shorter welding times and highest RS (P08 and P12), the SZ/ TMAZ interface is poorly consolidated (Fig. 3), and provides little structural integrity to the weld, contributing to low ULSF measured for these parameters, discussed in



**Fig. 2** Micrograph of RFSSW cross-Sect. (3 s welding time, 1500 rpm RS, 2.25 mm plunge depth) highlighting stir zone (SZ), thermo-mechanical affected zone (TMAZ), heat affected zone (HAZ) and typical defects: a) tunnel defect, b) lack of mixing, c) curved hook feature

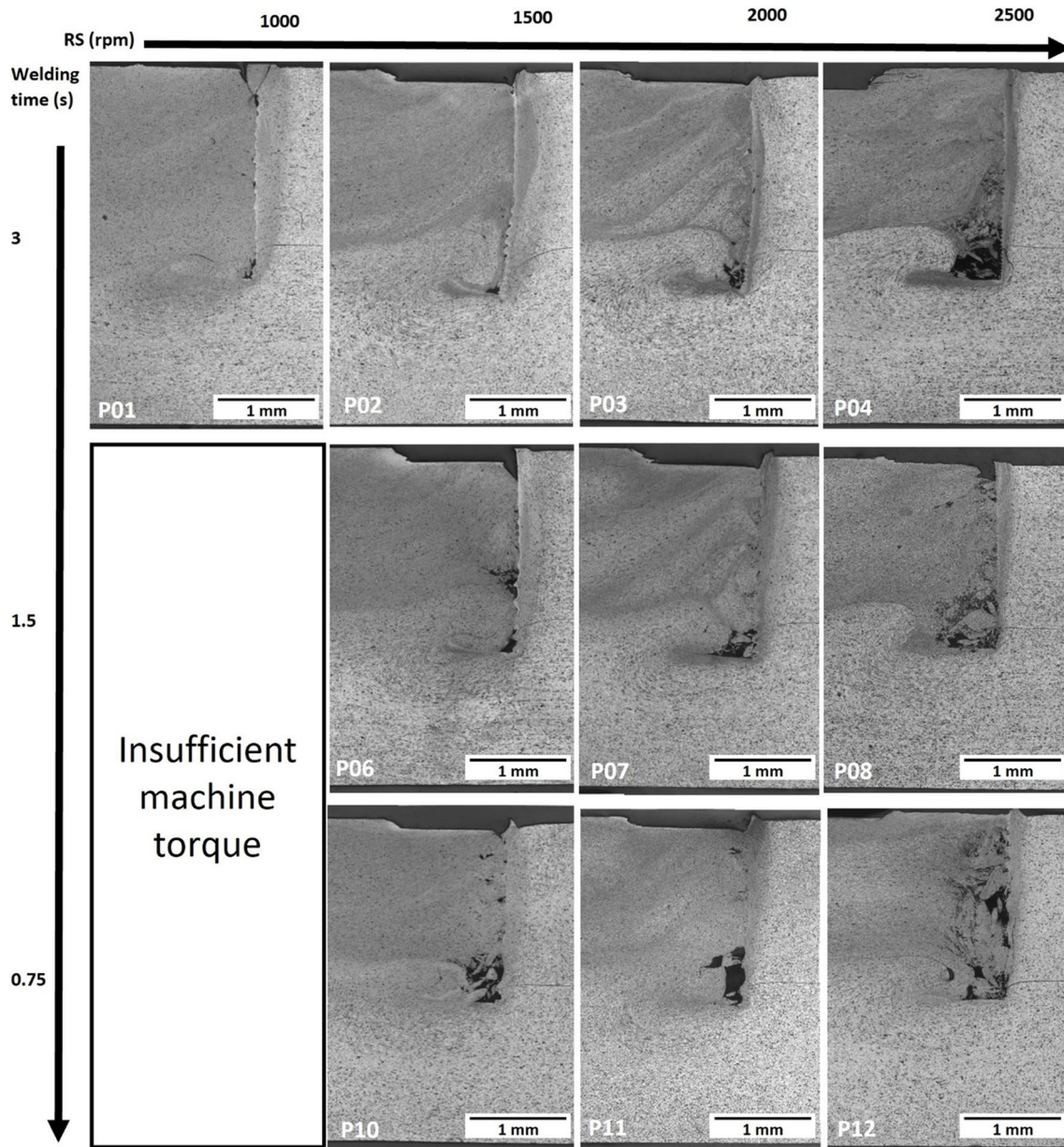


**Fig. 3** Micrographs through centre of welds for all welding parameters, showing region of defect formation

Sect. 3.3. The formation of these defects is due to a lack of heat input as the welding time is reduced, resulting in material that cannot flow back into the shoulder region during the refill stage. Similar results have been reported by other groups [2, 40].

### 3.1.2 Mixing defects

Figure 4 presents micrographs of lap interfaces (Fig. 4a-c), and SZ/ TMAZ interfaces (Fig. 4d-f) of welds produced at 2000 rpm RS and varying welding times. Overall, it can be seen that reducing welding time led to poorer quality

mixing at both interfaces. For 3 s welds, full mixing at the lap interface is evident from the gradual transition in grain structure from fine and equiaxed in the SZ, to the coarser structure of the bottom sheet, with no visible joining seam (Fig. 4a). Similarly, at the SZ/TMAZ interface (Fig. 4d), thorough mixing is evident from the consistent structure of fine equiaxed grains across the interface (indicated by the white dashed line). At 1.5 s welding time, the transition in grain structure at the lap interface is more abrupt (Fig. 4b), indicating less vigorous mixing between the top and bottom sheet. This transition disappears altogether at 0.75 s welding time, as evidenced in Fig. 4c by the immediate transition



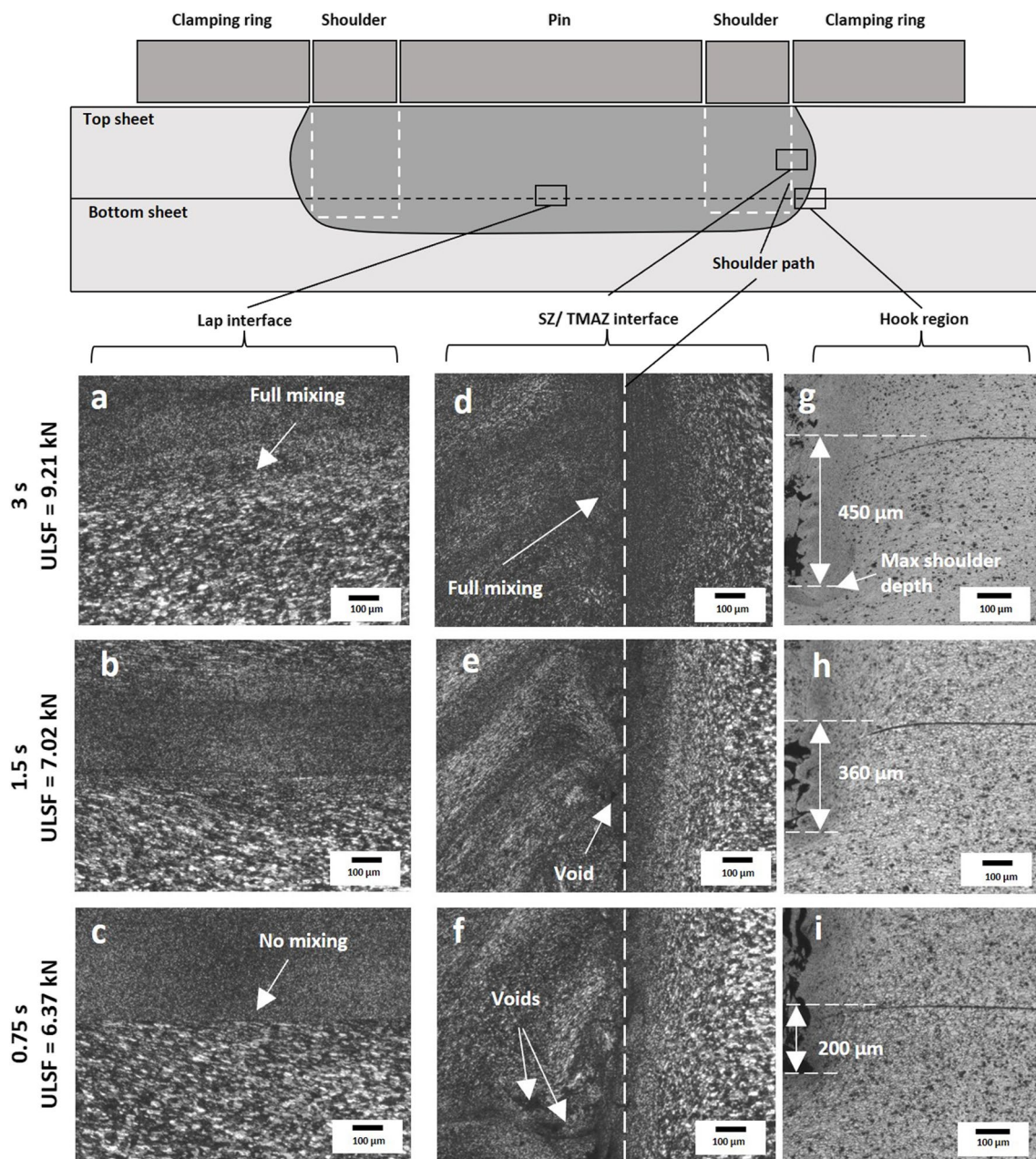


**Fig. 4** Etched micrographs of key locations within welds produced at 2000 rpm RS with different welding times, **a** full weld of parameter set P03, **b-e** SZ lap interfaces, **f-i** SZ/ TMAZ interfaces, **j-m** hook region

from fine, equiaxed grains in the top sheet, to coarse and directional grains in the bottom sheet, similar to those of the bulk material. An inhomogeneous grain structure (fine and coarse bands) is visible at the SZ/TMAZ interface of 1.5 s and 0.75 s welds, and voids can be identified along the shoulder plunge path (Fig. 4e,f). Although no existing literature has characterised defect formation at such short welding times, the present results are consistent with trends observed at conventional welding times [2, 40]. It is proposed herein that poor material flowability brought about by insufficient

heat generation is the primary driver of defect formation at short welding times. Attempting to increase heat generation by increasing RS did not improve weld quality, and resulted in poorer mixing and greater defect formation, as shown in Fig. 3 – P08, P12. Gerlich et al. [41] discussed this phenomenon in depth in the context of friction stir spot welding; they concluded that increasing RS can inhibit mixing by promoting slippage at the tool/workpiece interface. Others have reported similar observations on the RFSSW process [2, 42].

### 3.1.3 Hook feature

The influence of short welding times on hook geometry can be seen in Fig. 4g-i. In all cases hooks slope in the downwards direction but become flatter as welding time is reduced (Fig. 4i). While a nominal plunge depth of 2.25 mm was specified for all welds in the current work (450 μm penetration into the bottom sheet), Fig. 4g-i show that this was actually achieved only for 3 s welds (Fig. 4g). In the case of 1.5 s (Fig. 4h) and 0.75 s (Fig. 4i) welds, penetration into the bottom sheet only reached 360 μm and 200 μm respectively, meaning plunge depth in fact reduced with welding time. This discrepancy is attributed to elasticity in components of the welding apparatus (backing anvil, frame etc.), coupled with the increased tool forces exerted when welding time is reduced [43]. The flattening of the hook is consistent with the findings of Li et al. [19], who reported that reducing plunge depth led to a flatter hook geometry.

### 3.2 Mechanical testing

As shown in Fig. 5 and Table 3, the ULSF achieved with all parameter sets exceeded the minimum value of 4.605 kN set by resistance spot welding standards [37]. For welds produced with welding times of 3 s, the ULSF exceeded the minimum requirements for comparable rivet joints of 7.27 kN [38]. The highest ULSF of 9.21 kN was achieved for parameter set P03 (RS of 2000 rpm and welding time of 3 s). Consistent with the findings of Shang et al. [29], these results demonstrate that lap-shear strength is not strongly correlated with void size, as both P01 and P02 produced welds with smaller tunnel defects (Fig. 3) yet had lower ULSF. ULSF is influenced more by the bonding quality of the SZ/TMAZ interface and the lap-interface, as discussed in Sect. 3.1.2. Overall, a positive relationship was found between ULSF and welding time, wherein higher welding times led to a higher ULSF at a given RS. An exception to

**Fig. 5** ULSF for welds produced at various RS and welding times, with a constant plunge depth of 2.25 mm

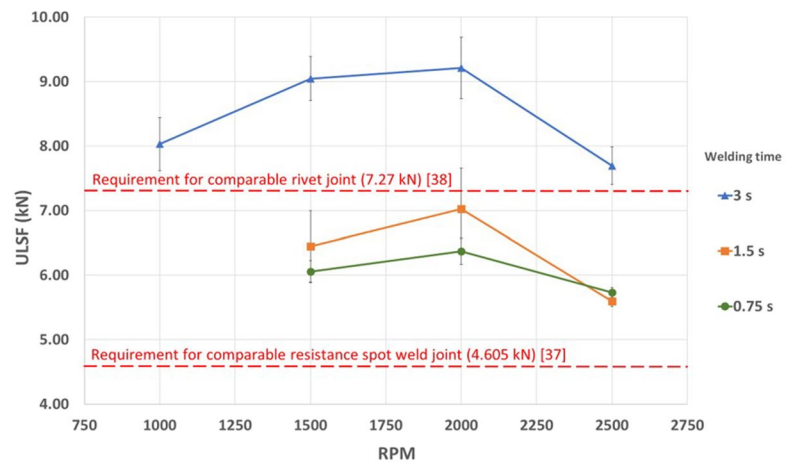


**Table 3** Results of lap shear testing

Parameter ID	Welding time (s)	RS (rpm)	Lap shear force (kN)	Standard deviation (kN)	Sample Failure mode		
					1	2	3
P01	3	1000	8.03	0.41	PPO	PPO	PPO
P02		1500	9.05	0.34	PPO	PPO	PPO
P03		2000	9.21	0.48	PPO	TWS	PPO
P04		2500	7.69	0.29	PPO	TLI	PPO
P05	1.5	1000	N/A	N/A	N/A	N/A	N/A
P06		1500	6.45	0.55	PPO	PPO	PPO
P07		2000	7.02	0.63	PPO	PPO	PPO
P08		2500	5.60	0.08	PPO	PPO	PPO
P09	0.75	1000	N/A	N/A	N/A	N/A	N/A
P10		1500	6.06	0.17	PPO	PPO	PPO
P11		2000	6.37	0.20	TWS	PPO	PPO
P12		2500	5.73	0.08	PPO	PPO	PPO

this trend was seen at 2500 rpm, where ULSF was slightly lower at a welding time of 1.5 s than 0.75 s.

At all welding times, ULSF increased with RS up to 2000 rpm, beyond which a sharp decrease was observed. As discussed in Sect. 3.1.2, higher RS has been shown to hinder the mixing process by promoting slippage at the tool interface. Li et al. [19] and Kluz et al. [44] presented similar findings for AA2024-T4 and AA7075-T6 respectively and attributed the effect to overheating of the workpiece material. The results presented in Fig. 5 are consistent with the findings of previous studies [18, 27, 30] that also achieved maximum ULSF at similar RS of 1900 rpm.

Despite the very short welding times used in this study, ULSF values are comparable with those reported in the literature for similar 2xxx series aluminium alloys. Figure 6 compares the results of the current work (RS = 2000 rpm) with existing literature in terms of welding time vs ULSF, showing that welding time has been reduced significantly with only modest reductions in weld strength.

### 3.2.1 Failure modes

The complex loading condition that arises during lap shear testing, with regions of tension and compression throughout the weld, resulted in three distinct failure modes: plug pull-out (PPO), 45° through the weld shear (TWS), and through the lap interface (TLI), as indicated in Fig. 7a.

Figure 7b-d show that the crack path for each failure mode begins in a similar manner. Firstly, a crack initiates at the hook tip on the tensile face of the weld (point 1). The crack then propagates upwards through the SZ/ TMAZ region to point 2 and around the circumference of the SZ towards point 3. As the crack propagates around the weld periphery, a moment acts about point 1 that causes a second crack to form at the hook tip on the opposing face (point 4). From this stage, the eventual failure mode is dictated by the weakest crack propagation path, either through the bottom sheet (PPO), through the lap interface (TLI), or through the

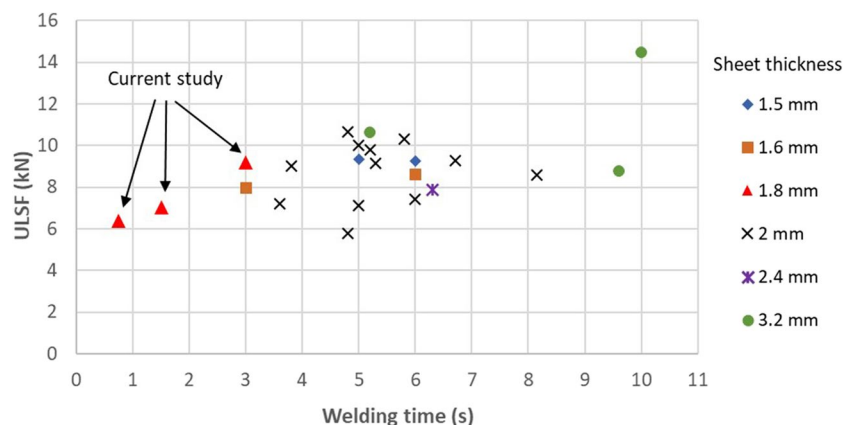
SZ (TWS). Similar failure modes have been reported extensively in previous studies [13, 18–21, 53, 54].

In the case of PPO failure (Fig. 7b i-ii), the initial crack continues to advance around the weld periphery in the top sheet to point 3. Simultaneously, the secondary crack advances downwards, towards the bottom weld face (point 6), and around the weld circumference to point 7. In this study, the presence of large tunnel defects promoted PPO failure in most cases by offering a weak crack propagation path towards the bottom face. Fractography of the failure surface (Fig. 7b ii-iii) shows the distinctive dimple rupture structure associated with tensile failure [19].

TLI failure occurs when a poorly bonded lap interface presents a weaker crack propagation path than through the bottom sheet. From Fig. 7c, it can be seen that the primary crack advances only partially around the weld periphery, while the secondary crack path can be traced from initiation at point 4, through the large tunnel defect (point 5–6) and directly through the lap interface to point 7. This is the result of partial bonding at the lap interface [13] (discussed in 3.1.2), as evidenced in Fig. 7c ii-iii where small islands of ductile dimple rupture can be identified within an otherwise unbonded region.

TWS failure (Fig. 7d) occurs when the SZ presents a weaker crack path than the bottom sheet or the lap interface. As the initial crack advances around the weld periphery, the area carrying the test load reduces and the stress at the compressive top face increases. Where no weaker path through the bottom sheet (leading to PPO) or the lap interface (leading to TLI) is available, a critical stress is eventually reached and a sudden shear fracture initiates at the compressive top face, propagating up through the SZ at approximately 45° [55]. The shear failure surface (Fig. 7d ii-iii) is distinguished by directional smearing and lack of ductile dimples. The magnified image in Fig. 7d i reveals the progression of an additional crack in the direction of the bottom sheet, indicating that this sample was nearing a PPO failure when the final shear fracture occurred. A comparison of the lap shear

**Fig. 6** Summary of published research for RFSSW joints of 2xxx aluminium, comparing lap shear strength vs welding time. Data is grouped according to the thickness of the welded sheets [18–29, 39, 45–52]





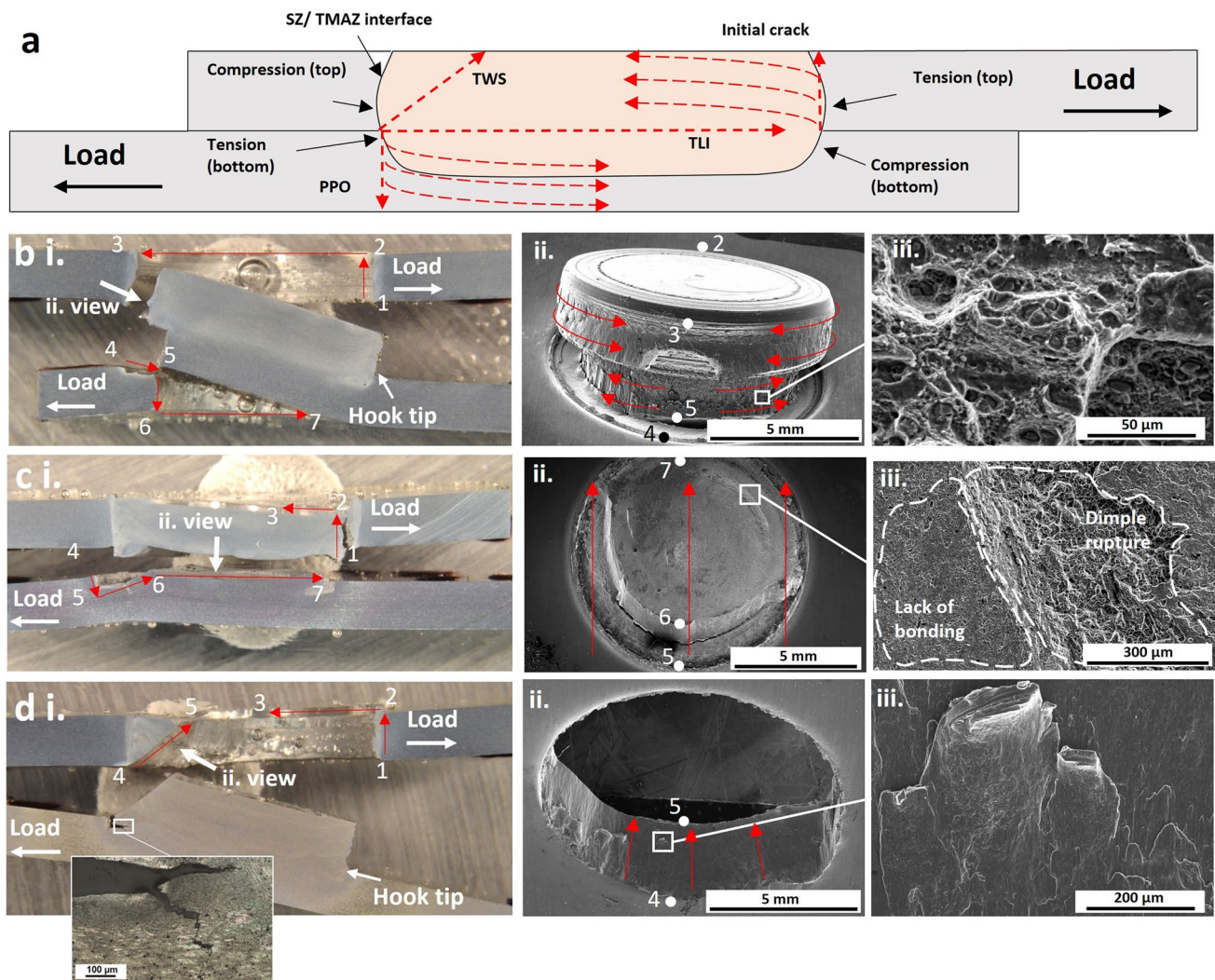


**Fig. 7** Examples of each failure mode a) weld cross section diagram, b) PPO (sample from set P11), c) TLI (sample from set P10), d) TWS (sample from set P03)

results and failure modes for each parameter set (Table 3) shows that there was no strong correlation between failure mode and weld strength, as PPO and TWS failures both occurred in samples with  $ULSF > 9$  kN and  $< 6.5$  kN.

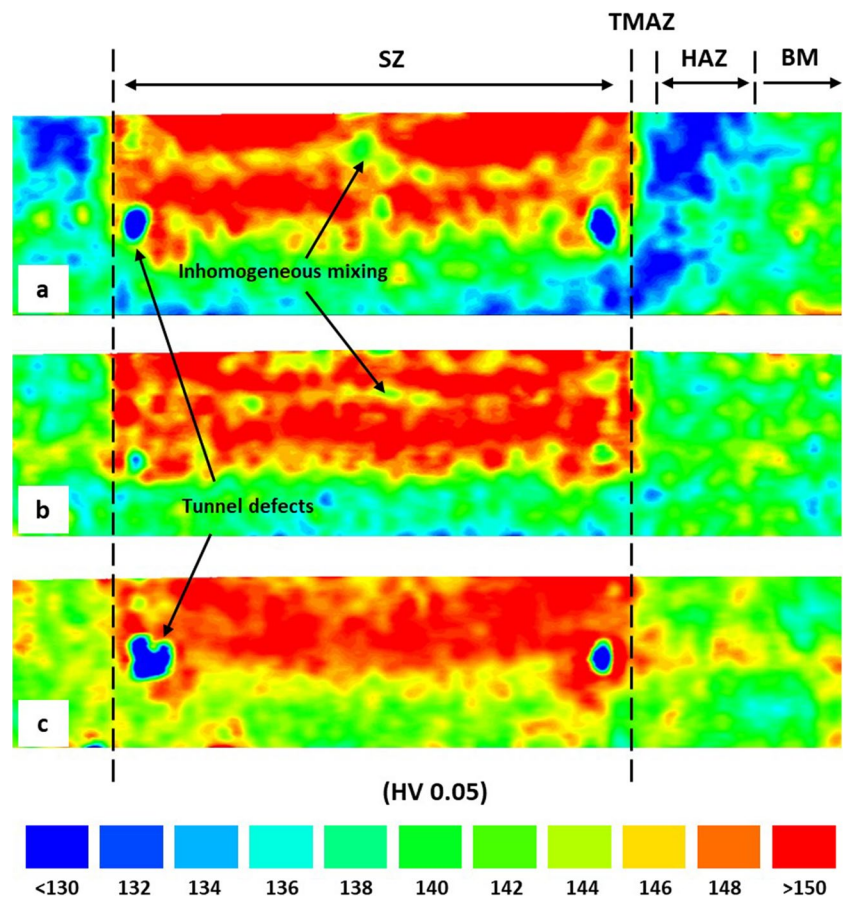
### 3.2.2 Microhardness mapping

Microhardness maps for welds produced at 2000 rpm RS and varying welding times are shown in Fig. 8. In comparison to the bulk material hardness (measured to be 138 HV), distinct regions of hardening and softening can be identified. Hardening within the SZ of approximately 15 HV is clear at all welding times (Fig. 8a-c), which can be attributed to the intense plastic deformation experienced within the SZ, and resultant fine grain structure and high dislocation density [56]. Small regions of slightly lower hardness are visible within the SZ of 3 s and 1.5 s welds, indicating

inhomogeneous mixing (Fig. 8a-b), however this fluctuation is very minor, in the range of only 5–10 HV.

Figure 8a shows that hardness begins to decrease at the SZ/TMAZ interface, and into the TMAZ where it is comparable to the bulk material. In this region, plastic deformation is limited compared to the SZ yet peak temperatures remain high, as demonstrated by Berger et al. [57]. Precipitation coarsening occurs with less of the deformation related hardening mentioned previously. In the case of the 3 s welds (Fig. 8a), an obvious HAZ can be seen surrounding the SZ where hardness drops to a minimum of around 125 HV. Prior research [2, 56] has addressed this phenomenon in more depth and attributed the softening to slight grain recovery and overaging of the bulk material. In contrast, neither the 1.5 s nor 0.75 s welds present any measurable softening characteristic of a HAZ (Fig. 8b-c). This can be attributed to very short exposure time of the workpiece to high

**Fig. 8** Microhardness maps through weld cross-section for welds produced at 2000 rpm RS and welding times of a) 3 s, b) 1.5 s, and c) 0.75 s



temperatures, and therefore less opportunity for heat affects to occur [58]. The similar hardness values in the TMAZ and the bulk material, coupled with the lack of an obvious HAZ makes it challenging to distinguish these different regions of the short duration welds using hardness mapping (Fig. 8b-c), however the presence of a TMAZ at all welding times is clearly shown in Fig. 4d-f.

## 4 Conclusions

This work has addressed a knowledge gap regarding the influence of short welding time on the defect formation, microstructure, mechanical properties, and failure modes of RFSSW AA2024-T3 joints. Welds were produced at welding times from 0.75 s—3 s, and RS of 1000 rpm—2500 rpm. Defects were observed at all process parameter combinations, with increasing severity across all RS as welding time decreased. Based on the results presented in this study, the following conclusions can be drawn:

1. Shorter welding times amplified defect formation, particularly tunnel defects, due to lack of heat generation and poor material flow, resulting in lower ULSF.
2. Increasing RS is not a viable mechanism of increasing heat generation, and actually exacerbates defect formation. Maximum ULSF was achieved with an RS of 2000 rpm at all welding times.
3. Welding times of 1.5 s and 0.75 s produced welds with no identifiable HAZ.
4. The highest ULSF was achieved when welding parameters resulted in a balance of good mixing at the SZ lap interface and at the SZ/ TMAZ interface.
5. Joints with static ULSF of 6.37 kN and 7.02 kN can be achieved at very fast welding times of 0.75 s and 1.5 s respectively, far faster than previously reported in the literature for 2xxx series aluminium RFSSW joints. This exceeds the static strength requirements of comparable resistance spot welding joints. At a welding time of 3 s, joints with static ULSF of 9.21 kN were achieved, exceeding requirements of comparable rivet joints.

Further process optimisation is required to eliminate weld defects at short welding times and will be the subject of future work.

**Acknowledgements** The authors gratefully acknowledge the financial support of the Scottish Association of Metals (charity number



SC014102) in partial funding of this work, as well as financial support from the Austrian aviation program “TAKEOFF” (PILOT, grant number 852796, 2018) and BMK—The Austrian Ministry for Climate Action, Environment, Energy, Mobility, Innovation and Technology. The authors would also like to acknowledge Magna for making available the joining equipment used in this work, as well as financial support from the University of Strathclyde and Technical University Graz within the Matched PhD programme framework.

**CRedit authorship contribution statement** **Jonathan Draper:** conceptualisation, methodology, formal analysis, investigation, writing – original draft, writing – review & editing. **Sebastian Fritsche:** conceptualisation, methodology, investigation, writing – review & editing. **Sergio T. Amancio-Filho:** conceptualisation, methodology, writing – review & editing, resources. **Alexander Galloway:** conceptualisation, methodology, writing – review & editing, resources. **Athanasios Toumpis:** conceptualisation, methodology, writing – review & editing, resources. **Andrew Garrick:** methodology, writing – review & editing.

**Data availability** Data will be made available on request.

## Declarations

**Competing interest** The authors have no competing interests to declare that are relevant to the content of this article.

**Open Access** This article is licensed under a Creative Commons Attribution 4.0 International License, which permits use, sharing, adaptation, distribution and reproduction in any medium or format, as long as you give appropriate credit to the original author(s) and the source, provide a link to the Creative Commons licence, and indicate if changes were made. The images or other third party material in this article are included in the article’s Creative Commons licence, unless indicated otherwise in a credit line to the material. If material is not included in the article’s Creative Commons licence and your intended use is not permitted by statutory regulation or exceeds the permitted use, you will need to obtain permission directly from the copyright holder. To view a copy of this licence, visit <http://creativecommons.org/licenses/by/4.0/>.

## References

- Feng XS, Bin Li S, Tang LN, Wang HM (2020) Refill Friction Stir Spot Welding of Similar and Dissimilar Alloys: A Review. *Acta Metall Sin English Lett* 33(1):30–42. <https://doi.org/10.1007/s40195-019-00982-4>
- Shen Z, Yang X, Zhang Z, Cui L, Li T (2013) Microstructure and failure mechanisms of refill friction stir spot welded 7075–T6 aluminum alloy joints. *Mater Des* 44:476–486. <https://doi.org/10.1016/j.matdes.2012.08.026>
- Hancock R (2004) Friction welding of aluminum cuts energy costs by 99%. *Weld J (Miami, Fla)* 83(2):40
- Ghaini FM, Sheikhi M, Torkamany MJ, Sabbaghzadeh J (2009) The relation between liquation and solidification cracks in pulsed laser welding of 2024 aluminium alloy. *Mater Sci Eng A* 519(1–2):167–171. <https://doi.org/10.1016/j.msea.2009.04.056>
- Sheikhi M, Ghaini FM, Torkamany MJ, Sabbaghzadeh J (2009) Characterisation of solidification cracking in pulsed Nd:YAG laser welding of 2024 aluminium alloy. *Sci Technol Weld Join* 14(2):161–165. <https://doi.org/10.1179/136217108X386554>
- Huang C, Cao G, Kou S (2004) Liquation cracking in partial penetration aluminium welds: Assessing tendencies to liquate, crack and backfill. *Sci Technol Weld Join* 9(2):149–157. <https://doi.org/10.1179/136217104225017071>
- Hosseini SA, Abdollah-zadeh A, Naffakh-Moosavy H, Mehri A (2019) Elimination of hot cracking in the electron beam welding of AA2024-T351 by controlling the welding speed and heat input. *J Manuf Process* 46(September):147–158. <https://doi.org/10.1016/j.jmapro.2019.09.003>
- Suryanarayanan R, Sridhar VG (2020) “Studies on the influence of process parameters in friction stir spot welded joints - A review. *Mater Today Proc* 37(Part 2):2695–2702. <https://doi.org/10.1016/j.matpr.2020.08.532>
- US Department of Transportation (2018) Advisory Circular: Corrosion Control for Aircraft
- Shen Z, Ding Y, Gerlich AP (2020) Advances in friction stir spot welding. *Crit Rev Solid State Mater Sci* 45(6):457–534. <https://doi.org/10.1080/10408436.2019.1671799>
- Zou Y, Li W, Shen Z, Su Y, Yang X (2023) Refill friction stir spot welding of aluminum alloys: State-of-the-art and Perspectives. *Weld World* 67(8):1853–1885. <https://doi.org/10.1007/s40194-023-01552-0>
- Larsen Y (2020) Brigham; Hovanski, “Reducing Cycle Times of Refill Friction Stir Spot Welding in Automotive Aluminum Alloys.” *SAE Tech Pap*. <https://doi.org/10.4271/2020-01-0224>
- Silva BH, Zepon G, Bolfarini C, dos Santos JF (2020) Refill friction stir spot welding of AA6082-T6 alloy: Hook defect formation and its influence on the mechanical properties and fracture behavior. *Mater Sci Eng A* 773(October 2019):138724. <https://doi.org/10.1016/j.msea.2019.138724>
- Gauthier E et al (2014) Numerical modeling of electrode degradation during resistance spot welding using CuCrZr electrodes. *J Mater Eng Perform* 23(5):1593–1599. <https://doi.org/10.1007/s11665-014-0908-9>
- Tier MD, Rosendo TS, Mazzaferro JA, Mazzaferro CP, dos Santos JF, Strohaecker TR (2017) The weld interface for friction spot welded 5052 aluminium alloy. *Int J Adv Manuf Technol* 90(1–4):267–276. <https://doi.org/10.1007/s00170-016-9370-1>
- Xu Z, Li Z, Ji S, Zhang L (2018) Refill friction stir spot welding of 5083-O aluminum alloy. *J Mater Sci Technol* 34(5):878–885. <https://doi.org/10.1016/j.jmst.2017.02.011>
- Cao JY, Wang M, Kong L, Guo LJ (2016) Hook formation and mechanical properties of friction spot welding in alloy 6061–T6. *J Mater Process Technol* 230:254–262. <https://doi.org/10.1016/j.jmatprotec.2015.11.026>
- Amancio-Filho ST, Camillo APC, Bergmann L, Dos Santos JF, Kury SE, Machado NGA (2011) Preliminary investigation of the microstructure and mechanical behaviour of 2024 aluminium alloy friction spot welds. *Mater Trans* 52(5):985–991. <https://doi.org/10.2320/matertrans.L-MZ201126>
- Li Z, Ji S, Ma Y, Chai P, Yue Y, Gao S (2016) Fracture mechanism of refill friction stir spot-welded 2024–T4 aluminum alloy. *Int J Adv Manuf Technol* 86(5–8):1925–1932. <https://doi.org/10.1007/s00170-015-8276-7>
- Li Z, Gao S, Ji S, Yue Y, Chai P (2016) Effect of Rotational Speed on Microstructure and Mechanical Properties of Refill Friction Stir Spot Welded 2024 Al Alloy. *J Mater Eng Perform* 25(4):1673–1682. <https://doi.org/10.1007/s11665-016-1999-2>
- de Sousa Santos P, McAndrew AR, Gandra J, Zhang X (2021) Refill friction stir spot welding of aerospace alloys in the presence of interfacial sealant. *Weld World* 1–21. <https://doi.org/10.1007/s40194-021-01113-3>
- Da Silva AAM, et al. (2007) Performance evaluation of 2-mm thick alclad AA2024 T3 aluminium alloy friction spot welding. doi: <https://doi.org/10.4271/2007-01-3812>
- Effertz PS, de Carvalho WS, Guimarães RPM, Saria G, Amancio-Filho ST (2022) Optimization of Refill Friction Stir Spot



- Welded AA2024-T3 Using Machine Learning. *Front Mater* 9:1–9. <https://doi.org/10.3389/fmats.2022.864187>
24. Zhang D, Xiong J, Ma Y, Jiang N, Li J (2022) Study of microstructure characteristics and corrosion behavior of 2524 aluminum alloy RFSSW joint. *Mater Charact* 190:112057. <https://doi.org/10.1016/j.matchar.2022.112057>
  25. Li G, Zhou L, Luo L, Wu X, Guo N (2019) Microstructural evolution and mechanical properties of refill friction stir spot welded alclad 2A12-T4 aluminum alloy. *J Mater Res Technol* 8(5):4115–4129. <https://doi.org/10.1016/j.jmrt.2019.07.021>
  26. Zou Y et al (2021) The impact of macro/microstructure features on the mechanical properties of refill friction stir spot-welded joints of AA2219 alloy with a large thickness ratio. *Int J Adv Manuf Technol* 112(11–12):3093–3103. <https://doi.org/10.1007/s00170-020-06504-2>
  27. Tier MD et al. (2008) The influence of weld microstructure on mechanical properties of alclad AA2024-T3 Friction Spot Welded. SAE Tech. Pap, no. 724. doi: <https://doi.org/10.4271/2008-01-2287>
  28. de Castro CC, Plaine AH, de Alcântara NG, dos Santos JF (2018) Taguchi approach for the optimization of refill friction stir spot welding parameters for AA2198-T8 aluminum alloy. *Int J Adv Manuf Technol* 99(5–8):1927–1936. <https://doi.org/10.1007/s00170-018-2609-2>
  29. Shang Z, Zuo Y, Ji S, Wang Y, Chai P (2021) Joint formation and mechanical properties of 2060 aluminum alloy refill friction stir spot welding joint. *Arch Metall Mater* 66(1):153–161. <https://doi.org/10.24425/amm.2021.134771>
  30. Parra B, Saccon VT, De Alcântara NG, Rosendo T, Dos Santos JF (2010) “An investigation on friction spot welding in AA6181-T4 alloy. 65th ABM Int Congr 18th IFHTSE Congr 1st TMS/ABM Int Mater Congr 2010 3:1861–1872. <https://doi.org/10.4322/tmm.2011.029>
  31. Hovanski Y, Curtis A, Michaelis S, Blackhurst P, Larsen B (2021) Advances in Refill Spot Welding Productivity. *Miner Met Mater Ser*, pp. 189–197. doi: [https://doi.org/10.1007/978-3-030-65265-4\\_18](https://doi.org/10.1007/978-3-030-65265-4_18)
  32. British Standards Institute (2019) Metallic materials. Tensile testing. Method of test at room temperature. London
  33. Li Y et al (2023) Effect of tool geometry on hook formation and mechanical properties of refill friction stir spot welding in alclad 2A12-T42 aluminium alloy. *Sci Technol Weld Join*. <https://doi.org/10.1080/13621718.2023.2180203>
  34. AMAG rolling GmbH (2006) Inspection certificate (EN 10204)
  35. British Standards Institute (2020) Metallic materials - Vickers hardness test BS EN ISO 6507–4:2018. London
  36. Kwee I, de Waele W, Faes K (2020) Weldability of high-strength aluminium alloy EN AW-7475-T761 sheets for aerospace applications, using refill friction stir spot welding. *Riv Ital della Saldatura* 72(3):259–276. <https://doi.org/10.1007/s40194-019-00732-1>
  37. British Standards Institution (2020) Welding for aerospace applications. Resistance spot and seam welding BS ISO 16338:2017. London
  38. US Federal Aviation Administration (2016) MMPDS-11: Metallic Materials Properties Development and Standardization (MMPDS)
  39. Yue Y, Shi Y, Ji S, Wang Y, Li Z (2017) Effect of Sleeve Plunge Depth on Microstructure and Mechanical Properties of Refill Friction Stir Spot Welding of 2198 Aluminum Alloy. *J Mater Eng Perform* 26(10):5064–5071. <https://doi.org/10.1007/s11665-017-2929-7>
  40. Adamus J, Adamus K (2019) The analysis of reasons for defects formation in aluminum joints created using RFSSW technology. *Manuf Lett* 21:35–40. <https://doi.org/10.1016/j.mfglet.2019.08.005>
  41. Gerlich A, Avramovic-Cingara G, North TH (2006) “Stir zone microstructure and strain rate during Al 7075–T6 friction stir spot welding. *Metall Mater Trans A Phys Metall Mater Sci* 37(9):2773–2786. <https://doi.org/10.1007/BF02586110>
  42. Rosendo T et al (2011) Mechanical and microstructural investigation of friction spot welded AA6181-T4 aluminium alloy. *Mater Des* 32(3):1094–1100. <https://doi.org/10.1016/j.matdes.2010.11.017>
  43. Su H, Wu CS, Pittner A, Rethmeier M (2013) Simultaneous measurement of tool torque, traverse force and axial force in friction stir welding. *J Manuf Process* 15(4):495–500. <https://doi.org/10.1016/j.jmapro.2013.09.001>
  44. Kluz R, Kubit A, Trzepiecinski T, Faes K (2019) Polyoptimisation of the refill friction stir spot welding parameters applied in joining 7075–T6 Alclad aluminium alloy sheets used in aircraft components. *Int J Adv Manuf Technol* 103(9–12):3443–3457. <https://doi.org/10.1007/s00170-019-03711-4>
  45. Schmal C, Meschut G, Buhl N (2019) Joining of high strength aluminum alloys by refill friction stir spot welding (III-1854-18). *Weld World* 63(2):541–550. <https://doi.org/10.1007/s40194-018-00690-0>
  46. Sun G et al (2023) Quality improvement of refill friction stir spot welds in 2A12-T42 aluminum alloy with alclad by adjusting sleeve design. *Int J Adv Manuf Technol* 130:1723–1734. <https://doi.org/10.1007/s00170-023-12834-8>
  47. Shi Y, Yue Y, Zhang L, Ji S, Wang Y (2018) Refill Friction Stir Spot Welding of 2198–T8 Aluminum Alloy. *Trans Indian Inst Met* 71(1):139–145. <https://doi.org/10.1007/s12666-017-1146-2>
  48. Pieta G, Dos Santos J, Strohaecker TR, Clarke T (2014) Optimization of friction spot welding process parameters for AA2198-T8 sheets. *Mater Manuf Process* 29(8):934–940. <https://doi.org/10.1080/10426914.2013.811727>
  49. Chai P, Wang Y (2019) Effect of Rotational Speed on Microstructure and Mechanical Properties of 2060 Aluminum Alloy RFSSW Joint. *Met Mater Int* 25(6):1574–1585. <https://doi.org/10.1007/s12540-019-00291-6>
  50. Wang Y, Chai P, Ma H, Cao X, Zhang Y (2020) Formation mechanism and fracture behavior in extra-filling refill friction stir spot weld for Al–Cu–Mg aluminum alloy. *J Mater Sci* 55(1):358–374. <https://doi.org/10.1007/s10853-019-03940-8>
  51. Zou Y et al (2022) Characterizations of dissimilar refill friction stir spot welding 2219 aluminum alloy joints of unequal thickness. *J Manuf Process* 79:91–101. <https://doi.org/10.1016/J.JMAPRO.2022.04.062>
  52. Wang Y, Chai P (2020) Effects of welding parameters on micro-junction structure and fracture behavior of refill friction stir spot welded joints for 2060 aluminum alloys. *Weld World* 64(12):2033–2051. <https://doi.org/10.1007/s40194-020-00981-5>
  53. Fritsche S, Draper J, Toumpis A, Galloway A, Amancio-Filho ST (2022) Refill friction stir spot welding of AlSi10Mg alloy produced by laser powder bed fusion to wrought AA7075-T6 alloy. *Manuf Lett* 34:78–81. <https://doi.org/10.1016/j.mfglet.2022.09.010>
  54. Shen Z et al (2020) Material flow during refill friction stir spot welded dissimilar Al alloys using a grooved tool. *J Manuf Process* 49:260–270. <https://doi.org/10.1016/j.jmapro.2019.11.029>
  55. Zhou L, Luo LY, Wang R, Zhang JB, Huang YX, Song XG (2018) Process Parameter Optimization in Refill Friction Spot Welding of 6061 Aluminum Alloys Using Response Surface Methodology. *J Mater Eng Perform* 27(8):4050–4058. <https://doi.org/10.1007/s11665-018-3472-x>
  56. Zhao Y, Dong C, Wang C, Miao S, Tan J, Yi Y (2020) Microstructures evolution in refill friction stir spot welding of al-zn-mg-cu alloy. *Metals (Basel)* 10(1):1–10. <https://doi.org/10.3390/met10010145>
  57. Berger E, Miles M, Curtis A, Blackhurst P, Hovanski Y (2022) 2D Axisymmetric modeling of refill friction stir spot welding and

- experimental validation. *J Manuf Mater Process* 6(4):89. <https://doi.org/10.3390/jmmp6040089>
58. Huda Z, Zaharinie T (2009) Kinetics of grain growth in 2024-T3: An aerospace aluminum alloy. *J Alloys Compd* 478(1–2):128–132. <https://doi.org/10.1016/j.jallcom.2008.11.071>

**Publisher's Note** Springer Nature remains neutral with regard to jurisdictional claims in published maps and institutional affiliations.